Sensors and Actuators Reports 5 (2023) 100155

Contents lists available at ScienceDirect

Sensors and Actuators Reports

journal homepage: www.sciencedirect.com/journal/sensors-and-actuators-reports

Development of a new Ni voltammetric sensor for hardened concrete conditions estimate

Ana Martínez-Ibernón [a,*], Isabel Gasch [a], Josep Lliso-Ferrando [a], Manuel Valcuende [b]

[a] Interuniversity Research Institute for Molecular Recognition and Technological Development (IDM), Universitat Politècnica de València, Universitat de València, Valencia 46022, Spain
[b] Department of Architectural Construction, Universitat Politècnica de València, Valencia 46022, Spain

ARTICLE INFO

Keywords:
Voltammetric sensors
Monitoring systems
Concrete durability
PCA models

ABSTRACT

Developing efficient monitoring systems to control reinforced concrete structures (RCS) is still an open research line in the building sector. Thus, in this work was proposed the novelty use of Ni voltammetric sensor to control the concrete conditions by means of PCA model. The efficiency of voltammetric sensors are verified in other sectors like food or wastewater treatment, where the sensors are used in liquid media, in the study was intended verify the high potential use of this sensors in porous materials such as concrete. With this purpouse the sensor response was characterized in three different concretes ($w/c = 0.6$, $w/c = 0.5$ and $w/c = 0.4$) and three different concrete conditions (water satured conditions, presence of chlorides and concrete carbonation). Then, was developed a PCA model, where was verified the capability of the sensor to classify the concrete state. The validation of the model pointed an acceptance range between 78.3% and 95.4% (with a 95% confidence index).

1. Introduction

Noble metals like Au or Pt present catalytic performance that can help to distinguish and very accurately estimate the presence of different species, which is why they are widely used as electrodes and electrochemical sensors [1–7]. However, as these raw materials have been exhausted in recent years, are expensive and their price continues to rise, the study of replacing these metals for other non-noble ones, which are suitably catalytic in nature and allow costs to lower, has proliferated in industry [8]. One of these metals is Ni [9–11].

Ni and its oxides are very important in practical terms in a wide range of technological applications: electrochemical sensors, secondary electrodes in batteries, electrolytic H production, organic compounds oxidation, etc. [12–18]. The literature contains a certain number of works that have studied the $Ni(OH)_2$/NiOOH reaction owing to the reversible nature of the process [19]. This reaction is complex and one that is presented within the range between H_2O oxidation and reduction curves. Under basic conditions, Ni is covered with a hydrated $Ni(OH)_2$ layer [19–21] that reacts, can lead to the REDOX Ni(II)/Ni(III) reaction, and different products form.

The fact that its performance in alkaline media has been widely studied, it is low-cost and catalytic in nature, and the REDOX Ni(II)/Ni (III) reaction is reversible [22–25], all make using Ni to manufacture voltammetric sensors to monitor RCS' state very interesting. This would allow the number of control points to increase in relation to the sensors manufactured with noble (more expensive) metals, improve the monitoring system's robustness, and facilitate developing simple estimation models by means of the reversible Ni(II)/Ni(III) reaction.

This study presents the bases for developing a novel system that would allow a Ni voltammetric sensor to be employed to determine concretes' state (*e.g.*, presence of chlorides, carbonation, variations in O_2 and H_2O availability in the porous network). This is a novel study because, although voltammetric sensors are widely utilised in solution [26,27], their use in concrete is scarce, if not non-existent.

Unlike other sensors that are more widespread in concrete, such as potentiometric sensors [7,28], dynamic electrochemical techniques are applied in voltammetric sensors, such as cyclic voltammetry (CV). In CV, a potential signal is applied that varies according to the triangular sawtooth pattern over time. If the reaction run with the species of interest is achieved when a given potential is reached, the response in the sensor's current can be characterised in the implied potentials zone. Thus reduce the effect of reactions overlapping that can occur in the case of sensors where the measured realiced is passive such as: potential sensors and galvanic sensors. Moreover with CV results, multivariate

* Corresponding author.
E-mail addresses: anmarib@arqt.upv.es (A. Martínez-Ibernón), igasch@mes.upv.es (I. Gasch), jollife2@alumni.upv.es (J. Lliso-Ferrando), mvalcuen@csa.upv.es (M. Valcuende).

https://doi.org/10.1016/j.snr.2023.100155
Received 23 March 2023; Received in revised form 20 April 2023; Accepted 27 April 2023
Available online 27 April 2023

analysis techniques can be applied [29], which would allow the largest possible amount of information to be acquired from a system with many variables by simplifying the sample space to a smaller sized one. In this way, more than one parameter of interest can be controlled with a single sensor, thus optimising the system from the point of view of both material and economic resources.

This work centres on studying and characterising the Ni voltammetric sensor to obtain information about the conditions of concrete left in different environments. With this purpose the response of the sensor embedded in concretes made of three different qualities and submitted to distinct environmental exposures was studied (Phase 1). After analysing the results, a model to determine concretes' state by means of a principal component analysis (PCA) was specified (Phase 2).

2. Materials and methods

2.1. Sensor system

2.1.1. Electrochemical techniques applied in the sensor

The CV and IS (Impedance Spectroscopy) techniques were applied with Autolab PGSTAT10. Data were collected by the Nova 1.11 software.

Both the CV and IS techniques were applied using the 3-electrode configuration, where the working electrode (WE) was the Ni sensor and stainless steel (SS) plates were used as the counterelectrode (CE). A saturated calomel electrode (SCE) was employed as the reference electrode (REF).

CV was applied within the potentials range at which the REDOX Ni (II)/Ni(III) pair reaction occurs (Eq. (1)), and where the oxidation and water reduction curves begin (a pH≈13) [17].

$$Ni(OH)_2 \leftrightarrow NiO(OH) + H^+ + e^- \quad (1)$$

The Ru value [30] was obtained by means of IS, which was employed to correct the ohmic drop effect in the voltagrams obtained with CV. The sweep frequencies range went from 100,000 Hz to 1,000 Hz. The sweep at high frequencies was justified by being similar to the simple Randles circuit (Rs-Rp/Cdl). The efficient value of the applied signal was 10 mV.

2.1.2. Sensors fabrication process

To manufacture the Ni electrode, Ni thread was used (99% purity and 1 mm diameter). The electric connection was made employing multifilar cable with Teflon casing. The connection between the cable and the metal was protected by a heat-shrink tube and epoxy resin (Fig. 1).

2.2. Experimental

In this experiment, concrete samples were employed that measured 4 × 4 × 16 cm^3. They were made of three different concrete types in which Ni sensors, along with the SS CE, had been embedded (Fig. 2-A).

Table 1 summarises the average surfaces of the employed Ni sensor, the CEs, and the surface area ratio average between the two (S_{CE}/S_{WE}).

The concretes employed to manufacture samples were those specified in Table 2.

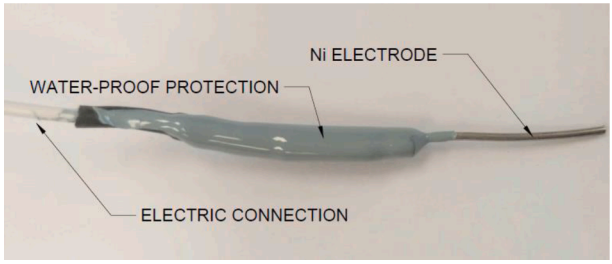

Fig. 1. Photograph of the Ni electrode.

For the study to offer statistical certainty for each dose, three batches were made. From each batch, two samples with sensors were manufactured. This totalled 18 samples. Therefore, 18 sensors were manufactured and 18 SS CEs were prepared.

2.2.1. Concrete characterisation tests

Characterisation standard tests specified in Table 3 were done of the studied concretes. The results of these standard tests were used to support the results obtained with the sensors.

2.2.2. Study variables and scenarios

This study was performed in two stages: the first one was when the influence of the sensor response was analysed owing to variations in O_2 availability and humidity; the other was when the influence of the presence of aggressive agents in concrete was analysed.

- Stage 1: influence of O_2 availability on the sensor's response. In this stage, samples were submitted to two different states:
  - Ambient conditions (ATM): a molar O_2 (x_{O2}) fraction of 0.21
  - Water saturation conditions (SAT): the O_2 availability in the concrete matrix was limited by the solution capacity of the gas in the concrete pore solution
- Stage 2: influence of the presence of aggressive agents in concrete on the response of the sensor. The samples employed in stage 1 were divided into two groups, where each one was submitted to a different aggressive atmosphere:
  - Carbonated concrete (CO_2)
  - Chloride attack (Cl^-)

In each state, measurements were repeated 4 times per sample until the statistical reliability of the results could be ensured. The weight of samples was measured every time they were tested.

2.2.2.1. Study under ambient conditions (ATM). After concreting samples, they were left in a curing chamber for 48 days at relative humidity (RH) close to 99%. Before tests began, all the samples were placed inside closed containers with saturated KCl solution to keep RH at 84.5 ± 0.3% [31]. The temperature conditions were those of the laboratory (T = 22 ± 3 °C). Sample carbonation was avoided under these conditions. Tests started when the variation in sample weight between two weighing sessions done on 2 consecutive days was below or equalled 2%.

2.2.2.2. Study under water saturation conditions (SAT). To accomplish the saturated state, all the samples were placed inside a vacuum chamber. The vacuum conditions inside the chamber continued for 1 h After this time, H_2O was allowed to enter until samples were completely immersed. The system was left for another hour without breaking the vacuum. After this time, the vacuum was broken. Samples were immersed for 48 h before running tests by applying electrochemical techniques.

2.2.2.3. Study under carbonation and chloride diffusion conditions. After performing the study under ambient and H_2O saturation conditions, samples were divided into two groups. Half the samples were placed inside an oven to be dried at 50 °C for 48 h After this time, all the samples were allowed to cool in the atmosphere for 24 h Then they were left inside a carbonation chamber at 3.5% (T = 23 ± 2 °C; HR≈60%). They remained under these conditions for 42 days and different degrees of carbonation according to concrete quality were obtained.

Bearing in mind the relation expressed in Eq. (2) and the test data, the carbonation constant (K_{CO2}, mm/year$^{1/2}$) was calculated for the 3.5% CO_2 concentration.

$$x = K * \sqrt{t} \quad (2)$$

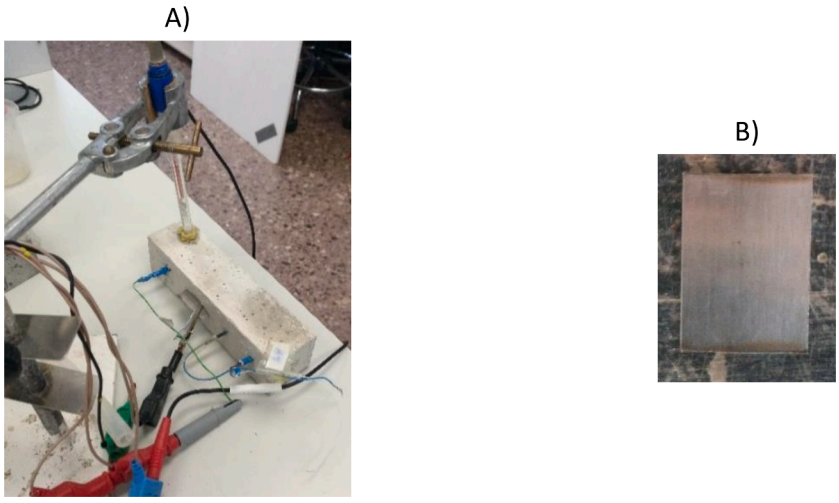

Fig. 2. A) Picture of the measurement time. B) Auxiliary stainless steel electrode.

Table 1
Summary of the average surfaces of the Ni sensors and of the CE made of SS plate.

Electrode		Surface (cm^2)	Surfaces ratio (S_{CE}/S_{WE})
WE	Ni	0.06±0.03	389.75
CE	SS PLATE	24.78±0.68	

Table 2
Quanties per m^3 of concrete.

MATERIALS	$kg/m^3_{of\ concrete}$ w/c = 0.6	w/c = 0.5	w/c = 0.4
Cement I 42.5 R-SR5	315	385	490
Water	189	193	196
Superplastifier	2.2	2.7	34
Silica sand	1212	1179	1115
Gravel	653	635	601

Table 3
Characterisation standard test performed.

Standard Test	Sampel shape	Total number of samples per concrete
Hardened concrete tests. Part 3. Determining samples' strength resistance (UNE 12,390–3:2009).	10 cm diameter, 20 cm high	6
Determining water absorption, density and accessible porosity for water (UNE 83,980:2014).	10 cm diameter, 5 cm high	3
Determining water penetration depth under pressure (UNE 83–309–90).	15 cm diameter, 30 cm high	3
Determining air permeability (UNE 83,981:2008).	15 cm diameter, 5 cm high	3
Determining electric resistivity (ρ): Direct method (reference method) (UNE 83,988–1:2008).	4 × 4 × 16 cm^3	3
Accelerated chloride diffusion test according to Standard NT-BUILD 492.	5 cm diameter, 10 cm high	6

where:

- x: penetration depth of the carbonation front (mm)
- K_{CO2}: carbonation constant ($mm/year^{1/2}$)
- t: time in which the carbonation front had advanced (years)

Fig. 3 shows the K_{CO2} values. According to these values, it was possible to evaluate the speed at which the studied concretes carbonated. That with the slowest velocity was the concrete with the lowest water/cement ratio, while that with the fastest velocity had the highest water/cement ratio.

The remaining samples were immersed in the 0.5 m NaCl solution. This concentration was selected for being that of seawater. Samples were left immersed in solution until tests ended.

2.2.3. PCA

The statistical PCA method was applied [6,32–36]. It allowed to simplify the complexity of the sample space so that it became a two-dimensional space to conserve the largest possible amount of information about the initial sample. That is, if j values were needed to characterise each sample, only two values were required. Both these new variables are known as a principal component (PC) [29,37]. The first PC (PC1) is selected in such a way that it contains maximum data variance. The second principal component (PC2) must contain the maximum of the remaining variance and be orthogonal to PC1. The representation on two axes allows samples to be easily grouped and classified.

This data processing protocol was applied by means of the Solo 9.0 computing tool (2022) (Eigenvector Research, Inc., Manson, WA USA 98,831; this software is available at http://www.eigenvector.com).

The matrix built with the testing data that was entered in the PCA tool is that which appears in Table 4. In this table, the samples column refers to the measurements taken per sample in each studied stage. The state column includes the name of the state which a sample corresponds to, along with concrete type. The variables columns contain all the CV data for the sweep 3 range and the Rs values.

The reference system obtained in the PCA was considered to be valid

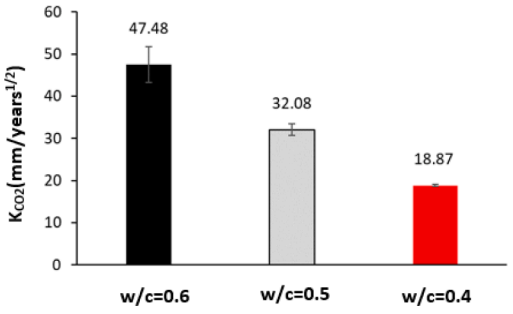

Fig. 3. Carbonation constant (K_{CO2}).

Table 4
Data table or matrix used in the PCA.

SAMPLES	STATE	Variable 1	.....	Variable j	Rs(Ω)
S1					
Sn					

provided that at least 80% variance was explained by the two principal components (PC1 and PC2).

2.3. Calibrating and validating the PCA model

To develop the model, it was necessary to follow calibration, fit and validation processes. During the fit process, any measurements that proved erroneous due to perturbations occurring while testing were removed. Even so, the size of samples and their variability were suitable to ensure the model's sufficient statistical reliability.

Fig. 4 summarises the sample size for calibrating and validating the PCA model. The samples employed in validation differed from those used in calibration.

In the validation of the PCA classification model, the confusion matrix (CM) was used, which is a typical classification model evaluation metric [38–41]. Therefore, to calculate the accuracy (ACC) of the model with respect to the three types of concrete, the type of confusion matrix shown in Table 5 was used.

The ACC [38–41] was calculated considering the Eq. (3) where TP is the number of true positives. The best accuracy is 1, and the worst is 0.

$$ACC = \frac{TP}{size\ sample} \tag{3}$$

3. Results and discussion

3.1. Results of the characterisation of concretes

Table 6 shows the average values obtained in the characterisation tests. It also shows the average coefficient of variation (Avrg Coef.V). Coef. V is defined as the quotient between standard deviation and the average value.

Bearing in mind the results of the characterisation tests, the indicators established by the French Civil Engineering Association (AFGC) [42] and concrete type according to EN 1992–1–1:2004 (EUROCODE2), we classify the employed concretes according to their potential durability as:

- Concretes with a low potential durability: w/c = 0.6 and w/c = 0.5.
- Concrete with a medium potential durability: w/c = 0.4.

Table 5
An example of a 3 × 3 confusion matrix.

		PREDICTED CLASS		
		A	B	C
ACTUAL CLASS	A	a	d	e
	B	f	b	g
	C	h	i	c

3.2. Characterisation of the response of the Ni electrode in hardened concrete (Phase 1)

In line with published works [30], the nomenclature employed in the voltagrams for the applied electric potentials were: ΔE_{RW} for the case in which the ohmic drop was not corrected; ΔE_{WE} for the case in which the ohmic drop was corrected. Moreover, the term i was used to refer to the response of the electric current in the CV test, and the term j to refer to the electric current value normalised by the WE surface, which is known as electric current density (μA/cm^2).

3.2.1. Comparison of voltagrams (solution vs. concrete)

Fig. 5 illustrates the voltagrams obtained in hardened concrete for normal pore solution conditions (pH≈12.5) and 60 days age. Two humidity conditions in the porous network were studied: H_2O saturation conditions (Fig. 5-A, SAT) and environmental conditions with high humidity (Fig. 5-B, ATM, ambient conditions $T = 22 \pm 3$ °C, HR≈70%). The four sweep ranges of potential defined in the experimental section were applied. Sweeps were sequentially applied one after another. Both voltagrams depict the typical Ni voltagram for an alkaline conditions [16,20], whose morphology coincides with that described by Vukovic [43]. The Ni oxides development zone is located between the H_2O oxidation and reduction curves. As the literature amply describes, a complex Ni(II)/Ni(III) reaction takes place in this zone [15,16,18,20].

Starting by describing the peaks identified in the voltagrams in Fig. 5, obtained in the anodic sense; that is, from left to right. Firstly, peak D is identified between potentials −1.1 V and −0.8 V. This is due to the transition of Ni^0 (active zones on the metal's surface) to $Ni(OH)_2$; that is, due to passive layer formation [15,16,18,20], whose reaction is described in Eq. (4). This peak appears when active zones remain on the metal's surface because, when Ni is placed in basic solution, the $Ni(OH)_2$ layer is spontaneously produced, which does not have to be uniform over the whole surface [19,44]. It also forms in free zones when the cathodic sweep of the H_2O reduction curve increases in line with what Sandoval, Schrebler and Gómez described [44].

$$Ni^0 + 2OH^- \leftrightarrow Ni(OH)_2 + 2e^- \tag{4}$$

Following the anodic direction, the zone lying between potentials −0.6 V and 0.3 V is due to the transformation of α- $Ni(OH)_2$ into β-$Ni(OH)_2$. The pair of REDOX A-a peaks observed within the 0.3 V and 0.7 V

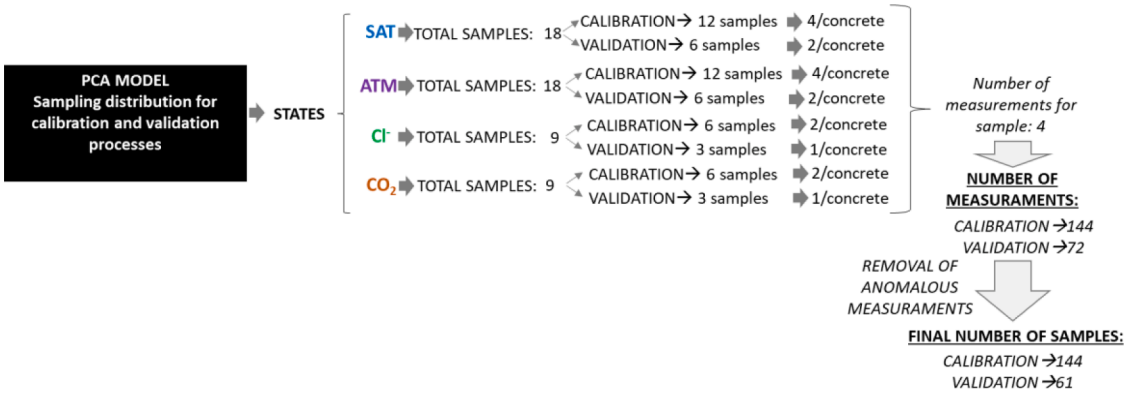

Fig. 4. Distribution of samples and sample size in the model to control concrete state for conventional concretes, PCA model.

Table 6
Average values of the characterisation tests done with the concrete used in Phase 2.

	$f_{c28days}$ (MPa)	% P.A.A.	% A.A.	P.A.P. (mm)	k ($x10^{-18}$ m^2)	ρ (Ωm)	D_{nssm} ($x10^{-12}m^2/s$)
w/c = 0.6	34.5	19.19%	7.59%	47	667.76	50.68	45.22
w/c = 0.5	42.9	17.21%	7.47%	26	521.37	52.38	25.35
w/c = 0.4	56.8	14.85%	6.65%	10	413.56	62.56	9.7
Avrg Coef.V	5.49%	7.47%	6.27%	11.20%	26%	11.38%	8.43%

Compression resistence at 28 days (fck28das) (UNE 12,390–3:2009),% accessible porosity for water (A.P.W.) and% water absorption (W.A.) (UNE 83,980), water penetration depth under pressure (P.D.P.) (UNE 83–309–90), air permeability coefficient (k) (UNE 83,981), electric resistivity (ρ) (UNE 83,988–1:2008), non-steady-state migration coefficient (Dnssm)(NT BUILD 492). [The coefficient of variation (Coef.V) is defined as the quotient between the standard deviation and the average value].

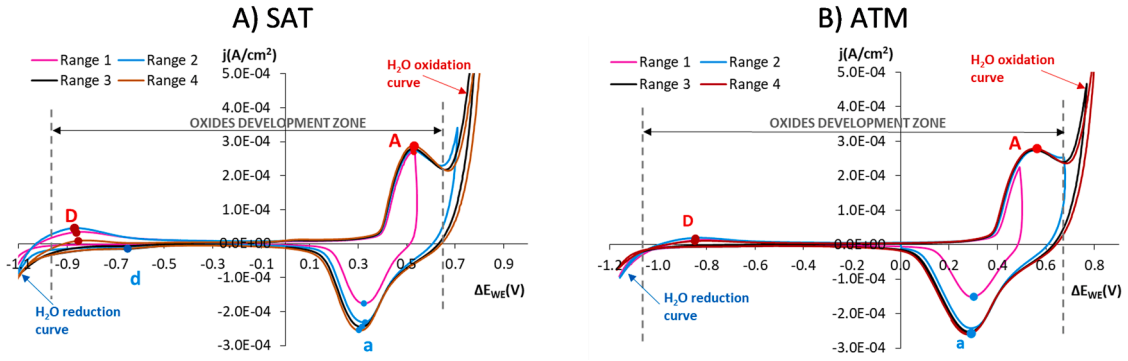

Fig. 5. A) Voltagrams obtained with the Ni sensor embedded in concrete w/c = 0.6 under water saturation conditions. B) Voltagrams obtained with the Ni sensor embedded in concrete w/c = 0.6 under ambient conditions.

range is associated with the REDOX $Ni(OH)_2$/NiOOH reaction (Eq. (5), for a basic medium).

$$Ni(OH)_2 + OH^- \leftrightarrow NiOOH + H_2O + e^- \quad (5)$$

Peak A is $Ni(OH)_2$ oxidation with NiOOH layers of different species forming, while peak a (cathodic sweep) is the inverse reduction reaction [15,16,18,20]. The j value of these peaks is affected by the sweep range, some authors point out that an increase in the j of peaks A-a is owing to the proliferation of other Ni oxide species that form during the H_2O oxidation curve [23,45,46].

When the voltagram is followed in the cathodic direction, a shoulder peak, cathodic peak d, sometimes appears in the potentials −0.8 V and −1.1 V zone, which is due to the passive $Ni(OH)_2$ layer [17]. Generally, however, the reduction in the passive layer occurs at very negative potentials when the sweep of the H_2O reduction curve considerably increases, and active zones of the metal are generated. In them, the anodic sweep once again forms an $Ni(OH)_2$ layer and peak D increases.

3.2.2. *Influence of humidity, chloride ions and concrete carbonation on the response of the Ni sensor*

Fig. 6 and Fig. 7 provide an example of the Ru value and the voltagram of all three concretes studied in this phase (w/c = 0.6, w/c = 0.5, w/c = 0.4), and also for the four concrete conditioning states: saturated H_2O state (SAT), atmospheric conditions (ATM), presence of chlorides (Cl^-) and carbonated state (CO_2). The objective of the comparison is to show how the sensor reacts to the different changes that might take place in concrete.

With all the concretes, when passing from state SAT to state ATM, and as H_2O availability diminishes, concrete's electric resistance increases, which gives way to a rise in Ru (Fig. 6-A). This means that Faraday processes (exchange of loads) are limited, and the response to electric current lowers in state ATM (Fig. 7-A, 7-C and 7-E). Besides, greater H_2O availability must favour the REDOX Ni(II)/Ni(III) process.

When both the ionic concentration in the concrete pore solution and H_2O availability increase, the concrete's Ru lowers more than in state SAT (Fig. 6-A). This is not the case of concrete w/c = 0.4 because chlorides did not diffuse up to the sensor's zone in this concrete during the study period. Fig. 8-A, 8-B and 8-C provide an example of a colorimetric evaluation by spraying $AgNO_3$.

Regarding the CV results (Fig. 7-A, 7-C and 7-E), new products were generated by the reaction of chlorides with $Ni(OH)_2$, as discussed in the study in solution section.

Finally for concrete carbonation (CO_2), in concretes w/c = 0.6 and w/c = 0.5 carbonation occurred all around the sensor, but it only

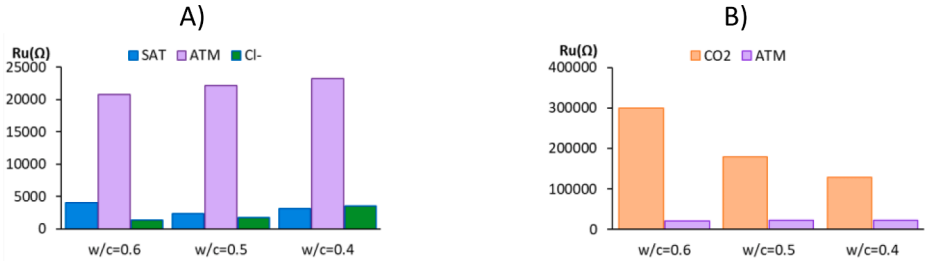

Fig. 6. Ru values for those tests whose voltagrams are shown in Fig. 7. A) concrete under water saturation (SAT), atmospheric (ATM) and chloride diffusion (Cl^-) conditions. B) concrete under atmospheric (ATM) and carbonated concrete (CO_2) conditions.

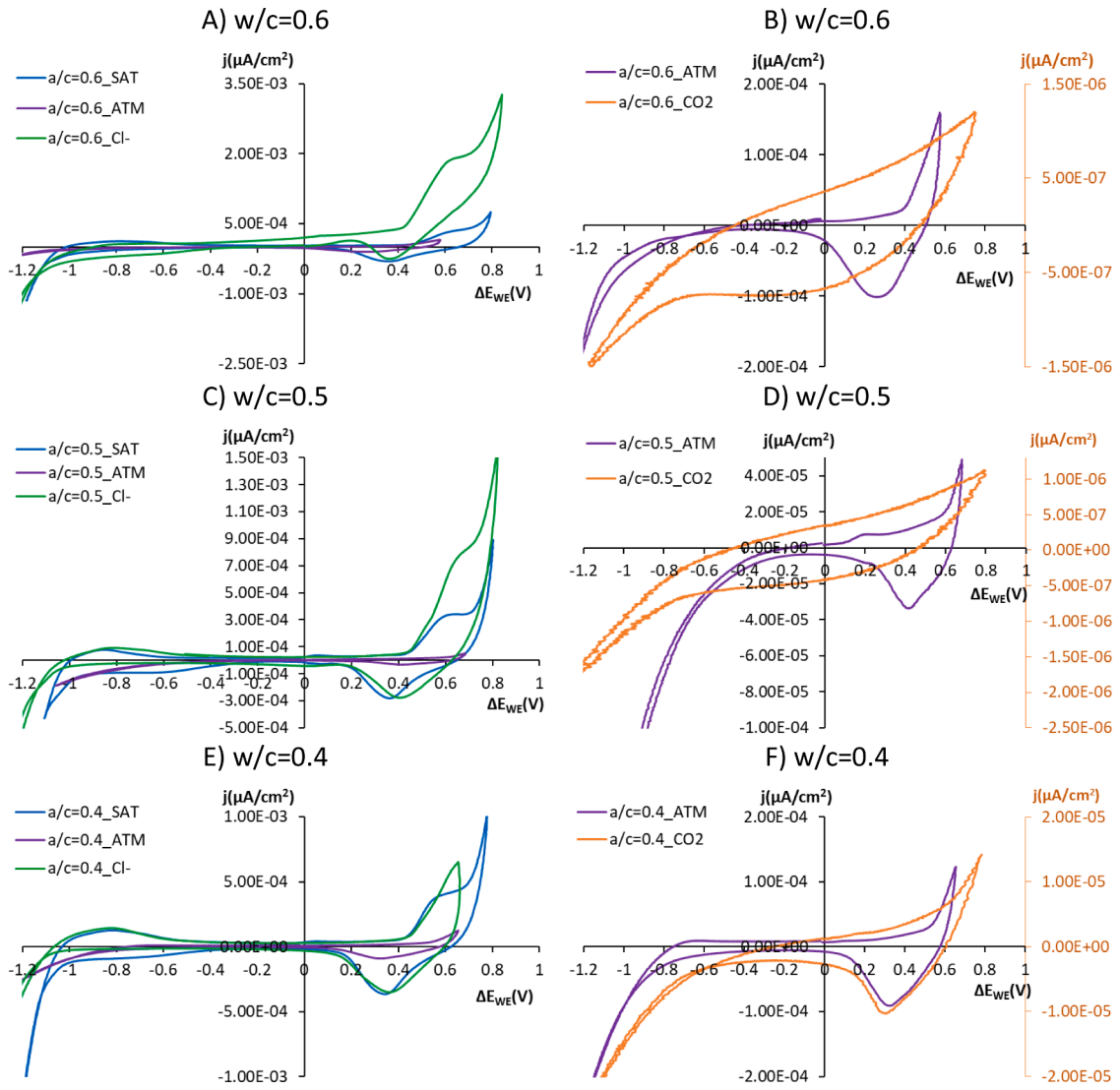

Fig. 7. A, C and E) The CV results obtained with the Ni sensor in concrete hardened under water saturation (SAT), atmospheric (ATM) and chloride diffusion (Cl^-) conditions. B, D and F) The CV results obtained with the Ni sensor in concrete hardened under atmospheric (ATM) and carbonated concrete (CO_2) conditions.

reached a depth of 0.5 cm in concrete w/c = 0.4 d Fig. 8-D, 8-E and 8-F illustrate an example of a colorimetric evaluation by spraying phenolphthalein.

In concretes w/c = 0.6 and w/c = 0.5, the stronger effect observed with the chosen sweep range, range 3, was the effect on the ohmic drop because the Ru value abruptly rise (Fig. 6-B). This is why the obtained electric current in the voltagram is very small. Thus when the resistance to ionic circulation increased, the circulation of the loads between the WE and the CE was lesser, and the pair of REDOX A-peaks could not be seen.

In concrete w/c = 0.4, the carbonation front did not reach the sensor's zone, but achieved a carbonation depth of 0.5 cm (Fig. 8-F), which affected the ionic circulation zone between the WE and the REF and, thus, Ru increased (Fig. 6-B). This is why differences are seen in the voltagram for state ATM.

3.3. Model of the concrete state classification. PCA model (Phase 2)

Fig. 9 includes the graph with not only the PCA scores, but also the distribution of the samples on the plane formed by the two PCs for all the concretes and in the five analysed states. PC1 is on the X axis and accounts for 99.73% of data variance, with PC2 on the Y axis accounting for 0.18% of data variance. The total data variance explained by both axes is 99.91%. Therefore, the PCA model well represents the information provided by the samples in calibration.

The samples employed for the PCA study of Fig. 9 are grouped according to both the state they were submitted to (SAT, ATM, $Cl^-$and CO_2) and concrete type (w/c = 0.6, w/c = 0.5 and w/c = 0.4). The PCA graph distinguishes the groups associated with each state, although the groups associated with states CO_2 and Cl^- are very close to groups ATM and SAT, respectively.

3.3.1. Detecting variations in humidity availability

The PCA scores graph (Fig. 9) indicates two grouping zones with well-differentiated dots, and appear on either side of the fucsia dashed line drawn in the graph. These two zones belong to different H_2O saturation states. On side Z1, the groups associated with the samples tested under NON—H_2O saturation conditions (ATM and CO_2) appear, while the groups of the samples tested under H_2O saturation conditions (SAT and Cl^-) are found on side Z2.

This indicates that as a dot appears further up in the graph and in a perpendicular direction to the fucsia dashed line, humidity availability is closer to the H_2O saturation state (a tendency marked by F-H_2O; Fig. 9).

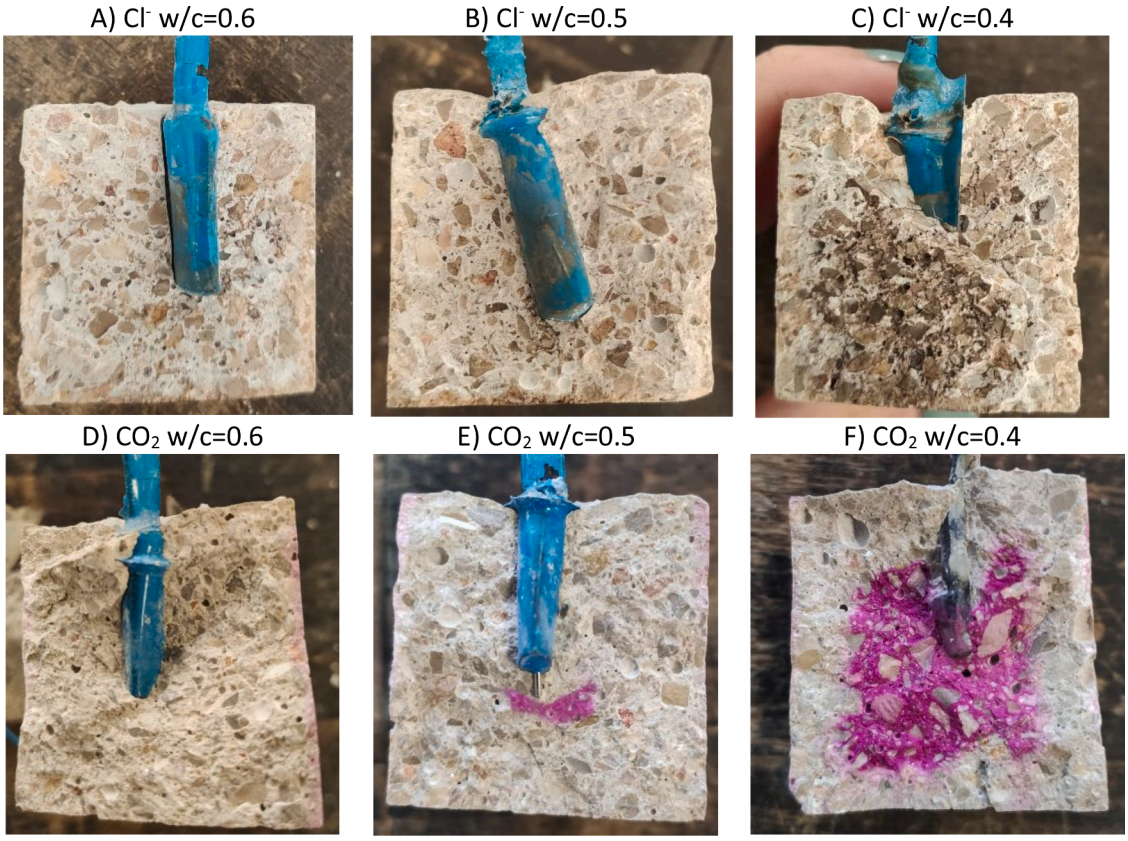

Fig. 8. A, B and C) Photographs taken of the samples sprayed with $AgNO_3$ after tests. D, E and F) Photographs taken of the samples sprayed with phenolphthalein after tests.

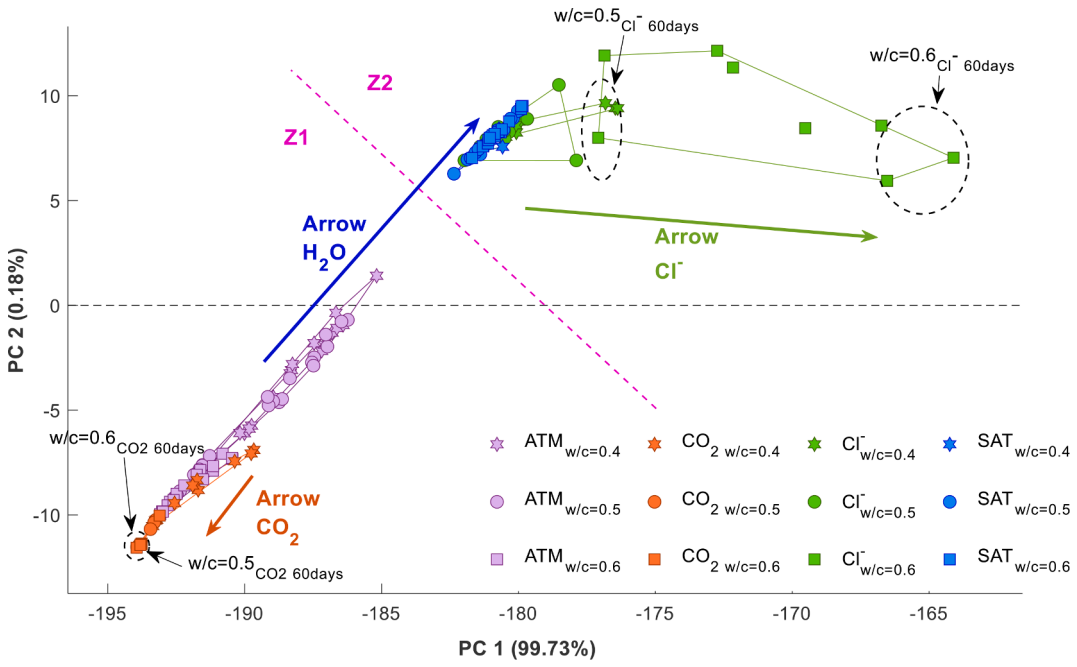

Fig. 9. PCA analysis graph for all the studied concretes and in all the tested states. Lilac: Atospheric air conditions (ATM); Orange: carbonated samples (CO_2); Green: samples immersed in 0.5 m NaCl (Cl-); Blue: water saturation conditions (SAT).

In the saturated state (SAT; blue), the groups of the different concretes overlap. Under such conditions, O_2 availability is low and, consequently, in this state (SAT) the kinetics of the REDOX Ni(II)/Ni(III) reaction is similar for the three studied concretes.

In Fig. 10, the PCA graph extends to the zone corresponding to the groups of states ATM and CO_2. In this extension, in the groups of dots associated with state ATM, the concrete w/c = 0.6 group is found and is further away from the H_2O saturation zone, while the concrete w/c =

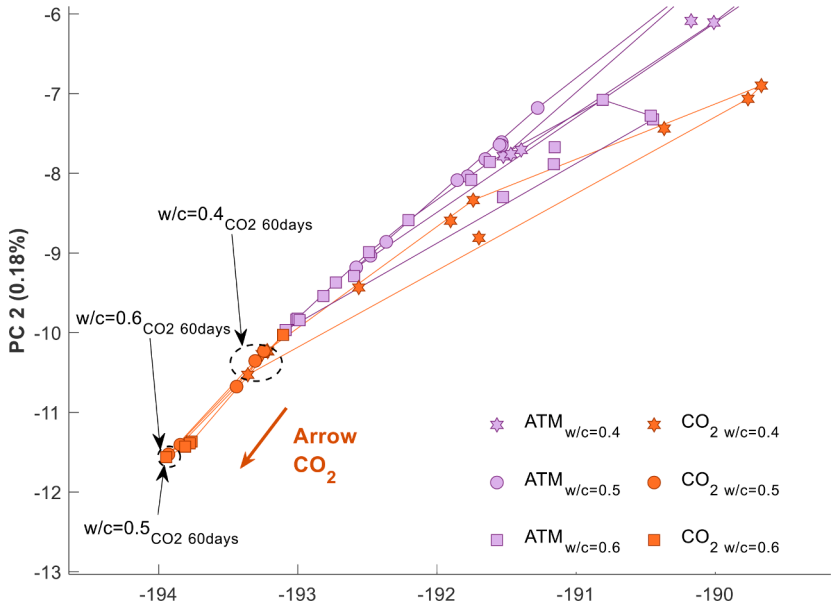

Fig. 10. Details of Fig. 9 in the carbonation groups zone (CO_2).

0.4 group is closer. According to the concrete characterisation results, concrete w/c = 0.6 presents more porosity and O_2 permeability. Thus in the matrix of this concrete, O_2 availability is greater and H_2O availability is lesser. This implies that the characterisation tests validate the marked H_2O availability in the graph with F-H_2O.

The capacity to distinguish a different H_2O availability is very interesting for not only studying the kinetics of corrosion processes in rebars, but also because it allows defects in their cover layers or the existence of cracks to be detected. The appearance of cracks may favour the mass penetration of both gases and liquids. So under these conditions, dots appear to be abnormally displaced in the PCA graph.

3.3.2. Cl^- detection

In Fig. 9, the groups of the dots associated with state Cl^- follow the tendency marked by arrow F_Cl^-. This tendency is in accordance with Cl^- availability in the concrete matrix because it is coherent with the D_{nssm} values and the chloride migration coefficient in the non-stationary state (Table 6). This coefficient is higher when concrete's resistance to chloride diffusion is lesser. As concrete w/c = 0.4 has the lowest D_{nssm} value and concrete w/c = 0.6 has the highest one, the tendency marked by F-Cl^- (Fig. 9) indicates that Cl^- presence is greater.

In concrete w/c = 0.6, the ordenated dispersion of dots occurs in direction F_Cl^-. It is a coincidence that the dots further away from the start of the arrow are those which correspond to a longer immersion time for the sample in 0.5 m NaCl solution. Given the effect of the gradient of concentrations between the concrete pore solution and the solution in which samples are immersed, the free chlorides concentration inside samples rises with time. This diffusion phenomenon occurs until the Cl- concentration of the concrete pore solution is balanced with the solution in which samples are immersed.

3.3.3. Concrete carbonation detection

The sensor is capable of detecting the variations caused by carbonation in the capillary network, by the concrete pore dissolution and its evolution with time (F-CO_2, Fig. 10). The groups of the dots associated with this state can be distinguished from those corresponding to the other states (Fig. 9).

This affirmation is validated by the correlation with the standardised test results:

- Bearing in mind concretes' carbonation constant (Fig. 3), the degree of carbonation for concrete w/c = 0.6 is higher than for concretes w/c = 0.5 and w/c = 0.4 during the study period. This is confirmed by the images in Fig. 8 where, after 60 carbonation days, the carbonation front in concrete w/c = 0.4 still does not reach the sensor. In the PCA graph (Fig. 10), it is possible to see how the dots that are associated with the last measurement taken in this state (at 60 days) are ordered from lower to higher concrete porosity in the F-CO_2 direction. This tendency, which is marked by F-CO_2, indicates a higher degree of carbonation in its direction
- With time, the carbonation front in concrete advances (the degree of concrete carbonation increases with time), which is reflected in the PCA. It shows how the dots further away from the start of the F-CO_2 of the group associated with each concrete are those that correspond to the measurements taken at 60 days when samples were left in the carbonation chamber (Fig. 10)
- As explained at the start of this section, total carbonation does not occur in concrete w/c = 0.4 in the zone where the sensor is found. However, the Ni sensor is capable of detecting the change that takes place around it when carbonation begins, and dots are displaced downwardly and to the left in relation to the corresponding dots in $ATM_{w/c\ =\ 0.4}$.

3.3.4. Validation model

After verifying the consistency of the results by making a comparison to the results of the standardised tests, the PCA model was validated. In Fig. 11, the validation data about the calibrated PCA are represented (V-ATM, V-CO_2, V-Cl^- and V-SAT). The zones corresponding to each state was defined by the calibrated model. The graph in Fig. 11 shows how most of the samples employed in the validation are represented in the zone that corresponds to the state in which the measurement was taken.

In order to obtain the accuracy of the model the information of the PCA validation graph is represented in 4 × 4 confusion matrix for state (Table 7). Furthermore, to evaluate the accuracy of the model by type of studied concrete, a 4 × 4 CM was defined for each studied concrete (Table 8).

According with the confusion matrix the accuracy of the model per concrete and overall is shown in the Table 9. The accuracy for the model is good being the value close to unit. Regarding to the results of ACC by concrete, the low value is obtained in w/c = 0.5, but this value close to 0.8 is consider acceptable as can be verified in bibliography [38,47].

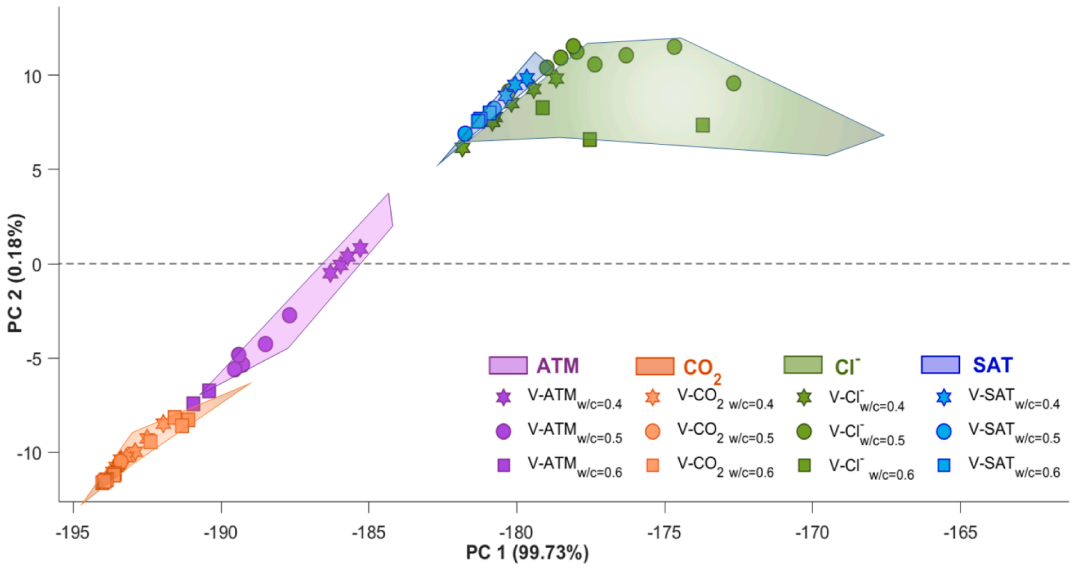

Fig. 11. Validation of the model to control RCS' durability (PCA model). Lilac: atmospheric conditions (ATM); Green: samples immersed in 0.5 m NaCl solution (Cl^-); Orange: carbonated samples (CO_2); Blue: water saturation conditions (SAT). The red circles on the dashed line indicate the values whose position is not coherent with the measurement conditions they belong to.

Table 7
4 × 4 confusion matrix for classes ATM, CO_2, Cl^- and SAT.

		Predicted Classification			
		ATM	CO_2	Cl^-	SAT
Actual Classification	ATM	9	2	0	0
	CO_2	0	23	0	0
	Cl^-	0	0	12	6
	SAT	0	0	0	9

The overall ACC expresses the hit percentage for the sample size, then the model confidence interval (CI) will be estimated with a confidence level of 95% (α), which is usual, accepting that the probability of being correct is distributed as the Binomial Function. The acceptance number is 53 samples out of the total number of 61, which corresponds to an acceptance rate ($\hat{p}$) of 86.9%. 8 samples out of 61 are rejected, which corresponds to a rejection rate ($\hat{q}$) of 13.3%.

Considering that $n * \hat{p} = 61 * 0.869 = 53.01 > 5$ and $n * \hat{q} = 61 * 0.133 = 7.99 > 5$, the Binomial Function, defined as B(n, $\hat{p}$)=(61, 0.869), can approach the Normal Distribution [48–50], N(n, $\sqrt{\frac{\hat{q}*\hat{p}}{n}}$)=(60, 0.0435), and CI is obtained with the equation below:

$$\left(\hat{p} - Z_{\frac{\alpha}{2}} \cdot \sqrt{\frac{\hat{q}\cdot\hat{p}}{n}}; \hat{p} + Z_{\frac{\alpha}{2}} \cdot \sqrt{\frac{\hat{q}\cdot\hat{p}}{n}}\right) \quad (6)$$

where $Z_{\alpha/2} = 1.96$. This is the value for $\alpha/2 = 0.025$.

It can be stated that, after the calculation, the CI for the model's probability of being correct is $p = 0.869 \pm 0.085$, which means that the real percentage of the model being correct at the 95% confidence level would lie between 78.3% and 95.4%.

Conclusions

Taking into account the previously presented analysis, the following conclusions are drawn:

- The performance of the sensor embedded in concrete is similar to the performance in solution, but with some differences in oxide layers formation due to the limitation in the diffusion or transport phenomena that take place in the hardened concrete matrices. In any case, the sensor reacts in concrete in the same way as in solution this favours the use of this sensor in porous materials.
- According to the results, the voltammetric Ni sensor, along with the applied electroanalytical techniques and the PCA analysis, allows the tested concrete state (presence of chlorides, concrete carbonation, and variations in O_2 and humidity in the porous network) to be distinguished
  - √ The sensor is capable of not only detecting variations in humidity availability, but of also showing the tendencies correlated to concrete porosity and its O_2 permeability
  - √ Although the sensor detects the presence of Cl^- anions, its sensitivity is low. It is impossible to detect variations complying with changes in the concentration of the anion inside the concrete matrix over time in concretes with low and medium porosity
  - √ The sensor detects the carbonation front. The response of the sensor changes as the carbonation front advances in the concrete

Table 9
Accuracy calculated values.

	overall	w/c = 0.4	w/c = 0.5	w/c = 0.6
ACC	0.869	0.950	0.792	0.941

Table 8
4 × 4 Confusion matrix for each concrete.

w/c = 0.4		Predicted Classification				w/c = 0.5		Predicted Classification				w/c = 0.6		Predicted Classification			
		ATM	CO_2	Cl^-	SAT			ATM	CO_2	Cl^-	SAT			ATM	CO_2	Cl^-	SAT
Actual Classification	ATM	4	0	0	0	Actual Classification	ATM	5	0	0	0	Actual Classification	ATM	1	1	0	0
	CO_2	0	7	0	0		CO_2	0	7	0	0		CO_2	0	9	0	0
	Cl^-	0	0	5	1		Cl^-	0	0	4	5		Cl^-	0	0	3	0
	SAT	0	0	0	3		SAT	0	0	0	3		SAT	0	0	0	3

matrix. This allows high degrees of carbonation to be detected coherently with concrete type

- The validation of the model with accuracy of 0.869 and a population range between 0.783 and 0.954 demonstrates the potentially of the model.

Declaration of Competing Interest

The authors declare that they have no known competing financial interests or personal relationships that could have appeared to influence the work reported in this paper.

Data availability

No data was used for the research described in the article.

Acknowledgments

The authors would like to express their gratitude to the Spanish Ministry of Science and Innovation for the pre-doctoral scholarship granted to Ana Martínez Ibernón (FPU 16/00723). To the authors thank the Spanish Government for the Grant PID2020-119744RB-C21 funded by MCIN/AEI/10.13039/501100011033

References

[1] Y. Xiao, H.-.X. Ju, H.-.Y. Chen, Hydrogen peroxide sensor based on horseradish peroxidase-labeled Au colloids immobilized on gold electrode surface by cysteamine monolayer, Anal. Chim. Acta [Internet] 391 (1) (1999 May) 73–82. Available from: https://linkinghub.elsevier.com/retrieve/pii/S0003267099001968.

[2] Y.L. Zheng, D. Mei, Y.-.X. Chen, S. Ye, The redox reaction of hydrogen peroxide at an Au(100) electrode: implications for oxygen reduction kinetics, Electrochem. Commun. [Internet] 39 (2014 Feb) 19–21. Available from: http://linkinghub.elsevier.com/retrieve/pii/S1388248113004608.

[3] A. Latus, M. Enache, E. Volanschi, Drug-GSH interaction on GSH-Au modified electrodes: a cyclic voltammetry and electrochemical impedance spectroscopy study, J. Electroanal. Chem. [Internet] 661 (1) (2011) 120–129, https://doi.org/10.1016/j.jelechem.2011.07.025. Available from:.

[4] L. Lvova, Electronic Tongue Principles and Applications in the Food Industry. Electronic Noses and Tongues in Food Science [Internet], Elsevier, 2016, pp. 151–160, https://doi.org/10.1016/B978-0-12-800243-8/00015-9. Available from:.

[5] I. Campos, R. Masot, M. Alcañiz, L. Gil, J. Soto, J.L. Vivancos, et al., Accurate concentration determination of anions nitrate, nitrite and chloride in minced meat using a voltammetric electronic tongue, Sens. Actuat. B Chem. [Internet] 149 (1) (2010 Aug) 71–78. Available from: https://linkinghub.elsevier.com/retrieve/pii/S0925400510005058.

[6] R Bataller Prats, Fabricación y Puesta a Punto De Una Nariz Electrónica Húmeda para La Detección De Gases y Vapores [Internet]. P.h.D. Thesis, Universitat Politècnica de València, València, Spain,. [Valencia (Spain)], 2017. Universitat Politècnica de ValènciaAvailable from: https://riunet.upv.es/handle/10251/89083.

[7] Z. Du, P. Wang, Z. Chen, D. Cui, Z. Jin, H Zhang, All-solid-state, long term stable, and embedded pH sensor for corrosion monitoring of concrete, J. Build. Eng. [Internet] 57 (July) (2022), 104978, https://doi.org/10.1016/j.jobe.2022.104978. Available from:.

[8] M. Fouladgar, A high sensitive square wave voltammetric sensor based on ZnO nanoparticle ionic liquid paste electrode for determination of benserazide in biological samples, Meas. J. Int. Meas. Confed. [Internet] 86 (2016) 141–147, https://doi.org/10.1016/j.measurement.2016.02.057. Available from:.

[9] M. Kovendhan, H. Kang, S. Jeong, J.S. Youn, I. Oh, Y.K. Park, et al., Study of stainless steel electrodes after electrochemical analysis in sea water condition, Environ. Res. [Internet] 173 (March) (2019) 549–555, https://doi.org/10.1016/j.envres.2019.03.069. Available from:.

[10] F. Bidault, D.J.L. Brett, P.H. Middleton, N. Abson, N.P. Brandon, A new application for nickel foam in alkaline fuel cells, Int. J. Hydrog. Energy [Internet] 34 (16) (2009 Aug) 6799–6808, https://doi.org/10.1016/j.ijhydene.2009.06.035. Available from:.

[11] Z. Tian, Y. Li, S. Li, S. Vute, J. Ji, Influence of particle morphology and concentration on the piezoresistivity of cement-based sensors with magneto-aligned nickel fillers, Meas. J. Int. Meas. Confed. [Internet] 187 (September 2021) (2022), 110194, https://doi.org/10.1016/j.measurement.2021.110194. Available from:.

[12] D.S. Hall, C. Bock, B.R. MacDougall, An oxalate method for measuring the surface area of nickel electrodes, J. Electrochem. Soc. [Internet] 161 (12) (2014 Sep 3) H787–H795. Available from: https://iopscience.iop.org/article/10.1149/2.0711412jes.

[13] S.B. Hall, E.A. Khudaish, A.L. Hart, Electrochemical oxidation of hydrogen peroxide at platinum electrodes. Part II: effect of potential, Electrochim. Acta [Internet] 43 (14–15) (1998 May) 2015–2024. Available from: http://linkinghub.elsevier.com/retrieve/pii/S0013468697101165.

[14] C.-.C. Hu, C.-.Y. Cheng, Anodic deposition of nickel oxides for the nickel-based batteries, J. Power Sources [Internet] 111 (1) (2002 Sep) 137–144. Available from: https://linkinghub.elsevier.com/retrieve/pii/S0378775302002963.

[15] T. Wen, C. Hu, Y. Li, The redox behavior of electroless Ni/PTFE deposits in KOH, J. Electrochem. Soc. [Internet] 140 (9) (1993 Sep 1) 2554–2558. Available from: https://iopscience.iop.org/article/10.1149/1.2220861.

[16] G. Barral, F. Njanjo-Eyoke, S. Maximovitch, Characterisation of the passive layer and of hydroxide deposits of nickel by impedance spectroscopy, Electrochim. Acta [Internet] 40 (17) (1995 Dec) 2815–2828. Available from: https://linkinghub.elsevier.com/retrieve/pii/001346869500274I.

[17] A. Seghiouer, J. Chevalet, A. Barhoun, F. Lantelme, Electrochemical oxidation of nickel in alkaline solutions: a voltammetric study and modelling, J. Electroanal. Chem. [Internet] 442 (1–2) (1998 Jan) 113–123. Available from: https://linkinghub.elsevier.com/retrieve/pii/S0022072897004981.

[18] J. Mun, M.-.J. Lee, J.-.W. Park, D-J Oh, D-Y Lee, S.-.G. Doo, Non-aqueous redox flow batteries with nickel and iron tris(2,2'-bipyridine) complex electrolyte, Electrochem Solid-State Lett. [Internet] 15 (6) (2012) A80. Available from: https://iopscience.iop.org/article/10.1149/2.033206esl.

[19] R.S. Schrebler Guzmán, J.R. Vilche, A.J. Arvía, Rate processes related to the hydrated nickel hydroxide electrode in alkaline solutions, J. Electrochem. Soc. [Internet] 125 (10) (1978 Oct 1) 1578–1587. Available from: https://iopscience.iop.org/article/10.1149/1.2131247.

[20] R.S. Schrebler Guzmán, J.R. Vilche, A.J. Arvía, The kinetics and mechanism of the nickel electrode—III. The potentiodynamic response of nickel electrodes in alkaline solutions in the potential region of Ni(OH)2 formation, Corros. Sci. [Internet] 18 (8) (1978 Jan) 765–778. Available from: https://linkinghub.elsevier.com/retrieve/pii/S0010938X78800948.

[21] M.L. Teijelo, J.R. Vilche, A.J. Arvía, The electroformation and electroreduction of anodic films formed on silver in 0.1M sodium hydroxide in the potential range of the Ag/Ag2O couple, J. Electroanal. Chem. Interfac. Electrochem. [Internet] 162 (1–2) (1984 Mar) 207–224. Available from: https://linkinghub.elsevier.com/retrieve/pii/S0022072884801655.

[22] J.B. Raoof, R. Ojani, S.R. Hosseini, An electrochemical investigation of methanol oxidation on nickel hydroxide nanoparticles, South Afr. J. Chem. [Internet] 66 (August 2013) (2013) 47–53. Available from: http://www.scielo.org.za/scielo.php?script=sci_arttext&pid=S0379-43502013000100013.

[23] B.E. Conway, P.L Bourgault, Electrochemistry of the nickel oxide electrode: part III. anodic polarization and self-discharge behavior, Can J Chem [Internet] 40 (8) (1962 Aug 1) 1690–1707. Available from: https://ccww.com.eg/wp-content/uploads/2021/06/9030Corrosion-Behavior-of-Nickel-Electrode-in-NaOH-Solution1071.pdf.

[24] W.G. Cook, R.P. Olive, Pourbaix diagrams for the nickel-water system extended to high-subcritical and low-supercritical conditions, Corros. Sci. [Internet] 58 (2012) 284–290, https://doi.org/10.1016/j.corsci.2012.02.007. Available from:.

[25] D.S. Hall, D.J. Lockwood, C. Bock, B.R. MacDougall, Nickel hydroxides and related materials: a review of their structures, synthesis and properties, Proc. R. Soc. A Math. Phys. Eng. Sci. [Internet] 471 (2174) (2015 Feb 8), 20140792. Available from: https://royalsocietypublishing.org/doi/10.1098/rspa.2014.0792.

[26] J. Bujes-Garrido, Arcos-Martínez MJ, Development of a wearable electrochemical sensor for voltammetric determination of chloride ions, Sens. Actuat., B Chem. [Internet]. 240 (2017) 224–228, https://doi.org/10.1016/j.snb.2016.08.119. Available from:.

[27] I Campos Sánchez, Sensores Electroquímicos Tipo Lengua Electrónica Voltamétrica Aplicados Al Control Medioambiental y a la Industria Alimentaria [Internet], Universitat Politècnica de València, [Valencia (Spain)], 2013. Available from: https://riunet.upv.es/handle/10251/28937.

[28] M.A. Climent-Llorca, E. Viqueira-Pérez, M.M. López-Atalaya, Embeddable Ag/AgCl sensors for in-situ monitoring chloride contents in concrete, Cem. Concr. Res. 26 (8) (1996) 1157–1161.

[29] H. Martens, M. Martens, Multivariate Analysis of Quality: An Introduction [Internet], Wiley, 2001. Available from: https://books.google.es/books?id=aqpoh41CjtEC.

[30] A. Martínez-Ibernón, J.E. Ramón, J.M. Gandía-Romero, I. Gasch, M. Valcuende, M. Alcañiz, et al., Characterization of electrochemical systems using potential step voltammetry. Part II: modeling of reversible systems, Electrochim. Acta [Internet] 328 (2019 Dec), 135111. Available from: https://linkinghub.elsevier.com/retrieve/pii/S0013468619319826.

[31] ASTM COMPASS ® Standard practice for maintaining constant relative humidity by means of. 2018;02(2012):2018.

[32] Serrano Pérez-Ràfols, Esteban Ariño, Díaz-Cruz, Voltammetric electronic tongues in food analysis, Sensors [Internet] 19 (19) (2019 Sep 30) 4261. Available from: https://www.mdpi.com/1424-8220/19/19/4261.

[33] M Alcañiz Fillol, Diseño de un Sistema de Lengua Electrónica Basado En Técnicas Electroquímicas Voltamétricas y Su Aplicación en el ámbito agroalimentario [Internet], Universitat Politècnica de València, [Valencia (Spain)], 2011. Available from: http://tdx.cesca.cat/handle/10803/34322.

[34] R. Todeschini, Data correlation, number of significant principal components and shape of molecules. The K correlation index, Anal. Chim. Acta [Internet] 348 (1–3) (1997 Aug) 419–430. Available from: https://linkinghub.elsevier.com/retrieve/pii/S0003267097002900.

[35] D. Ballabio, A MATLAB toolbox for principal component analysis and unsupervised exploration of data structure, Chemom. Intell. Lab. Syst. [Internet] 149 (2015 Dec) 1–9, https://doi.org/10.1016/j.chemolab.2015.10.003. Available from:.
[36] G. Ivosev, L. Burton, R. Bonner, Dimensionality reduction and visualization in principal component analysis, Anal. Chem. [Internet]. 80 (13) (2008 Jul 1) 4933–4944. Available from: https://pubs.acs.org/doi/10.1021/ac800110w.
[37] Llecha J.B., Blanchar X.C. Diseño de una Nariz Electrónica Para la Determinación no Destructiva del Grado De Maduración de la Fruta [Internet]. UNIVERSITAT POLITÉCNICA DE CATALUNYA; Available from: https://www.tdx.cat/bitstream/handle/10803/6877/TESI_TEXT_COMPLET.pdf.
[38] Ž. Vujović, Classification model evaluation metrics, Int. J. Adv. Comput. Sci. Appl. 12 (6) (2021) 599–606.
[39] S. Ruuska, W. Hämäläinen, S. Kajava, M. Mughal, P. Matilainen, J. Mononen, Evaluation of the confusion matrix method in the validation of an automated system for measuring feeding behaviour of cattle, Behav. Processes. [Internet] 148 (March 2017) (2018) 56–62, https://doi.org/10.1016/j.beproc.2018.01.004. Available from:.
[40] M. Solla, B. Riveiro, Non-destructive techniques for the evaluation of structures and infrastructure, Non-Destruct. Techn. Eval. Struct. Infrastruct. (2016) 1–388.
[41] M.M. Manjurul Islam, J.M Kim, Vision-based autonomous crack detection of concrete structures using a fully convolutional encoder–decoder network, Sensors (Switzerland) 19 (19) (2019) 1–12.
[42] (France) G de travail M de grandeurs associées à la durabilité des bétons, Groupe de travail Mesure de grandeurs associées à la durabilité des bétons (France), Groupe de travail Conception des bétons pour une durée de vie donnée des ouvrages - Indicateurs de durabilité (France) V. Baroghel-Bouny, J. Jacob, Conception Des Bétons Pour Une Durée De Vie Donnée Des ouvrages: Maîtrise De La Durabilité Vis-À-Vis De La Corrosion Des Armatures Et De L'alcali-Réaction [Internet], AFGC, 2004 [Bagneux] (c/o SETRA, 46 Av. Aristide-Briand, 92225 Cedex)(Documents scientifiques et techniques - Association française de génie civil). Available from: https://books.google.es/books?id=YuobcgAACAAJ.
[43] M. Vuković, Voltammetry and anodic stability of a hydrous oxide film on a nickel electrode in alkaline solution, J. Appl. Electrochem. [Internet] 24 (9) (1994 Sep) 878–882. Available from: http://link.springer.com/10.1007/BF00348775.
[44] R. Sandoval, R. Schrebler, H. Gómez, Current peak multiplicity related to the Ni/Ni(OH)2 electrode, J. Electroanal. Chem. Interfac. Electrochem. [Internet] 210 (2) (1986 Oct) 287–294. Available from: https://linkinghub.elsevier.com/retrieve/pii/0022072886805812.
[45] G. Bronoel, J. Reby, Mechanism of oxygen evolution in basic medium at a nickel electrode, Electrochim. Acta [Internet] 25 (7) (1980 Jul) 973–976. Available from: https://linkinghub.elsevier.com/retrieve/pii/0013468680871027.
[46] M. KIBRIA, Electrochemical studies of the nickel electrode for the oxygen evolution reaction, Int. J. Hydrog. Energy [Internet] 21 (3) (1996 Mar) 179–182. Available from: https://linkinghub.elsevier.com/retrieve/pii/0360319995000666.
[47] A. Tharwat, Classification assessment methods, Appl. Comput. Informatics 17 (1) (2018) 168–192.
[48] H.J. Chang, M.C Lee, Applying computer simulation to analyze the normal approximation of binomial distribution, J. Comput. 28 (5) (2017) 116–131.
[49] L. Hodges, Common univariate distributions. Methods in Experimental Physics [Internet], Elsevier Masson SAS, 1994, pp. 35–61, https://doi.org/10.1016/S0076-695X(08)60252-5. Available from:.
[50] C. Tsokos, R Wooten, Normal probability. The Joy of Finite Mathematics [Internet], Elsevier, 2016, pp. 231–263. Available from: https://linkinghub.elsevier.com/retrieve/pii/B9780128029671000073.